On the characterization of microstructural characteristics and mechanical behaviour of mortar modified by flax fibre residues

Lotfi Hedjazi, Nicolas Stephant, Sofiane Guessasma

Construction and Building Materials 458 (2025) 139618

Contents lists available at ScienceDirect

Construction and Building Materials

journal homepage: www.elsevier.com/locate/conbuildmat

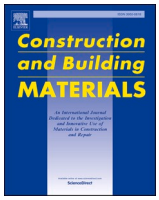

On the characterization of microstructural characteristics and mechanical behaviour of mortar modified by flax fibre residues

Lotfi Hedjazi [a], Nicolas Stephant [b], Sofiane Guessasma [c,*]

[a] ESTP Campus de Troyes, 1 Rue Fernand Sastre, Rosières-prés-Troyes 10430, France
[b] Nantes Université, CNRS, Institut des Matériaux Jean Rouxel, IMN, Nantes, France
[c] INRAE, Research Unit BIA UR1268, Rue Geraudiere, Nantes F-44316, France

ARTICLE INFO

Keywords:
Flax residues
Modified mortar
Mechanical performance
X-ray μ-tomography

ABSTRACT

In this study, we explore how the addition of flax fibre residues affects the microstructure and mechanical properties of modified mortars. Flax fibre residues from the individualization process are considered as fillers. Various formulations of mortar are adjusted by incorporating different proportions and sizes of flax fibre residues. The workability of fresh modified mortars is assessed through flow table experiments. X-ray μ-tomography is employed to investigate microstructural changes, focusing on pore content and the 3D spatial arrangement and content of natural residues. Mechanical performance is evaluated through compression tests conducted at different curing times. The findings indicate that flax residues can serve as effective substitutes, resulting in moderate loss in mechanical strength if the particle size is kept below 3 mm. Optimal formulations are found to require sieving of residues particle sizes resulting in small particles of 1 mm for an overall weight content of 5 % in the total weight of the cement used in the mix. These results demonstrate superior mechanical performance compared to all other tested conditions within only 7 curing days.

1. Introduction

The integration of natural fibres into civil engineering applications has garnered increasing attention due to their abundance, renewability, and favourable environmental footprint [1–5]. With growing concerns over the environmental impact of the construction sector [6,7], a shift towards more sustainable practices in building design, material selection, and cost evaluation has become essential [8,9]. Numerous studies highlight the significant CO_2 emissions from the built environment [10–14]. The introduction of natural fibres into cementitious matrices represents an important step towards reducing the ecological footprint of construction materials, despite the technical limitations posed by their weaker bonding capabilities compared to synthetic fibres. Natural fibres are derived from either plant (vegetal) or animal sources, and they are widely used in textiles, construction, and other industries due to their sustainability and eco-friendliness [15]. Plant-based fibres, also known as cellulosic fibres, include cotton, flax (linen), hemp, jute, and sisal. These fibres are extracted from various parts of plants, such as seeds, stems, and leaves, and are valued for their strength, biodegradability, and versatility [16]. However, using natural fibres derived from plants as reinforcement or substitutes in cementitious matrices presents significant challenges. Their irregular shape, variable dimensions, surface flaws, and hierarchical internal microstructure often result in lower mechanical performance compared to synthetic fibres [17]. Additionally, the moisture sensitivity of natural fibres can prolong setting times and complicate drying kinetics [18,19]. The processability of cementitious mixtures containing natural fibres also requires a rethinking of construction standards [20]. Additionally, issues such as odours and discomfort need to be addressed in building specifications. Despite these challenges, recent research has demonstrated successful attempts to incorporate natural fibres into cementitious materials [21,22]. For instance, Niyasom et al. [23] explored the use of natural fibres like banana and water hyacinth fibres, demonstrating their potential in eco-friendly concrete construction. Moreover, Pacheco-Torgal et al. [1] examined the integration of vegetable fibres into cementitious materials, emphasizing their capacity to reduce the carbon footprint of buildings. These results confirm that using natural fibres, such as flax, presents significant environmental potential, even if mechanical challenges remain. Furthermore, Marvila et al. [24] demonstrated that incorporating industrial residues, such as granite waste, can enhance the mechanical properties of cementitious mortars, further validating the use of flax residues in cementitious matrices

* Corresponding author.
E-mail address: sofiane.guessasma@inrae.fr (S. Guessasma).

https://doi.org/10.1016/j.conbuildmat.2024.139618
Received 8 August 2024; Received in revised form 3 November 2024; Accepted 15 December 2024
Available online 26 December 2024

2. State of the art

The use of plant fibres in construction materials presents challenges, particularly in terms of processing and fiber-matrix adhesion. For example, Fidelis et al. [25] investigated the interface characteristics of jute fibers in cementitious matrices, highlighting the bonding challenges between plant fibers and cement. These challenges are also relevant for flax fibers, which share structural similarities with other natural fibers used in construction materials. Additionally, Mosaberpanah et al. [26] explored the use of biochar and sewage sludge ash as partial cement replacements, demonstrating that bio-based fillers can improve compressive strength and durability. These findings align with the growing trend of using environmentally friendly solutions to maintain the mechanical integrity of construction materials while reducing their environmental impact. Moreover, Ghalieh et al. [27] conducted an experimental study on wrapping concrete columns with hemp fiber-reinforced polymer, revealing the mechanical reinforcement potential of natural fibers in structural applications. Finally, Prakash et al. [28] examined the mechanical characteristics of self-compacting concrete reinforced with roselle fibers, combined with supplementary cementitious materials like fly ash and metakaolin, offering insights into innovative combinations of natural fibers. From a mechanical standpoint, a primary argument favouring the use of plant fibres is their low material density, enabling the attainment of high specific properties [15–18]. For instance, the specific Young's modulus of natural fibres, particularly flax, rivals that of glass and steel fibres [19–22]. In various studies pertaining to civil engineering applications, the modified cementitious material's density is presented as a result of weight adjustments due to filler incorporation [23,24]. However, few studies prioritize a positive carbon footprint as an objective, which explains the lack of adequate attention to substituting cement with natural fibres [1].

Flax fibres, derived from the stem of the flax plant (Linum usitatissimum) [16,29]. Historically utilized for textiles and linens, flax fibres are increasingly gaining attention in modern industries such as automotive, aerospace, and construction for their remarkable mechanical properties and environmental sustainability [30]. These fibres boast high tensile strength and stiffness, making them ideal reinforcements in composite materials, including biodegradable plastics and bio-based composites, contributing to lightweight and eco-friendly solutions [31]. The main components of flax fibres are: cellulose (60–85 %), hemicellulose (9–21 %), with some residues of pectin (<7 %) and lignin (<5 %) [16]. The mechanical properties of flax fibres are typically assessed through tensile loading, where significant variation is observed due to defects and inherent variability in the fibres. For example, Young's modulus can range from 45 to 70 GPa, while tensile strength varies between 850 and 1400 MPa [16]. With ongoing research and development focusing on optimizing processing techniques and exploring novel applications, flax fibres continue to emerge as a promising eco-friendly alternative in various industries, especially in construction sector [32–34].

Much of the literature on flax fibre reinforcement in cementitious composites underscores the necessity for compromise in processing to address the inherent challenges of utilizing natural fibres [35–37].

These studies underscore the need to balance desired properties (e.g., thermal insulation versus structural integrity) when adjusting flax content in cementitious composites. Fibre content and dimensions emerge as crucial parameters for modulating composite properties [30,31]. Despite these adjustments, achieving superior mechanical performance often requires chemical modification of the fibres themselves to enhance cellulose properties, albeit at a cost and with environmental trade-offs [38,39]. Recent contributions advocate for the use of additives to enhance durability and mechanical performance in flax-reinforced resins in construction sector [34].

Aligned with this perspective, this study investigates the potential use of flax as a filler in cementitious materials. Due to the present pressure on the flax fibre supplying chain, this study focuses on the residues of the flax fibre transformation process. By targeting residues, the present study does not intend to promote conflicting usage of flax, and at the same time it maintains a high ambition of improving the environmental footprint of cementitious materials at the lowest possible cost. Thus, this study provides a quantitative evaluation of the mechanical performance of modified mortar incorporating flax residues according to different contents and sizes. The study compares all modified mortars, through compressive experiments over a 28-day curing period and provide microstructural interpretation based on synchrotron radiation X-ray microtomography experiments conducted at ESRF (Grenoble, France). X-ray microtomography is a powerful, non-destructive imaging technique used to analyse the internal microstructure of cementitious materials [40], particularly in distinguishing between open and closed porosity [41]. It is used in this study to derive quantitative and quantitative data about the content and spatial distributions of the phases in the modified mortars including flax residues and porosities.

3. Experimental layout

3.1. Materials and processes

The cement utilized in this investigation is CEM I/52.5, sourced from Ciment Calcia. In accordance with EN 197–1 standards, CEM I is an ordinary Portland cement with a clinker content exceeding 95 %, containing no significant amount of slag (0–5 % minor additional constituents). The cementitious matrix also incorporates standardized sand, a dry siliceous natural sand calibrated to 0/2 mm and meeting EN 196–1 specifications.

The cementitious matrix also incorporates standardized sand, a dry siliceous natural sand calibrated to 0/2 mm and meeting EN 196–1 specifications.

The biomass residues are considered as additives, which means that these do not replace any of the existing components in the mortar composition. Flax fibre residues provided by Eco-Technilin company (Valliquerville, France), France, undergo no chemical treatment (Fig. 1). Standard fillers are acquired by sieving techniques according to different meshes. The sieving of the flax residues is carried out to guarantee the uniformity of the dimensions of the fillers used in the formulation of the modified mortar (Fig. 1). A sieving equipment from 3 R is used with typical 3.15 mm, 2 mm, 1 mm meshes. Three flax residue sizes are used as fillers as well as the as-received residues without sieving (Fig. 1).

The primary aspect ratio of the residues (the ratio between length

Fig. 1. Optical micrographs showing morphology of studied flax residues.

and largest transverse dimension) varies considerably due to the variability in lateral dimensions of fibres. Optical imaging of a statistically representative flax residues is conducted. 2D image processing is conducted to determine some of the morphological descriptors such as the aspect ratio. ImageJ software (NIH, USA) is used for all processing operations. After converting the acquired images into 8 bit (256 grey level) images, threshold operation is conducted to isolate the residues from the background after carefully dispersing the residues to avoid clustering. From this preliminary optical imaging result, and across the considered sizes, the aspect ratio of flax residues ranges from 0.30 to 0.80 determined. Additionally, flax residues exhibit a solidity (the ratio between surface area and convex area) of 0.86 ± 0.10, as part of the optical imaging analysis, which is determined from 4 batches of residues containing more than 110 residues. Preliminary SEM observations are conducted to quantify the contamination with minerals. The percentage of residues is kept constant in the formulation, with a rate of 5 wt%. This amount is added to the cement. This large filler content is achieved for all sizes with no particular limitations in processability. Table 1 provides a summary of all attempted formulations.

Wet flax residues are added without soaking based on prior research demonstrating the advantageous effects of utilizing moist natural fibres on the mechanical performance of modified mortar. Flax is added to the mixing water, adhering to weight ratio guidelines for sand, water, and cement.

The reference mortar, devoid of any additives, is prepared according to the European classification under standard Norm NF EN: 196–1 [42]. Following this standard (Fig. 2), the cement-to-sand (C/S) weight ratio is 1:3, and the water-to-cement (W/C) ratio is 1:2. Each batch of three test specimens comprises 450 ± 2 g of cement, 1350 ± 5 g of sand, and 225 ± 1 g of water. The mortar is poured into right-prism moulds with dimensions of 4 × 4 × 16 cm^3. As shown in Fig. 2, two separations were added in the mould to achieve 4 cm^3 cubes for compression testing. During the first 24 h, moulds are stored in climatic chamber (AHC500)

Table 1
Characterization results for modified mortars as a function of the curing time. t_c: Curing time, D_f: Flax residue diameter; ρ_0: Density after 24 h; ρ_f: final density; ω_f: workability; σ_R: compression strength.

Sample	D_f (mm)	ω (%)	t_c (days)	ρ_0 (g/cm^3)	ρ_f (g/cm^3)	σ_R (MPa)
FD0	-	16.05	7	2.29	2.33	27.7
140		± 1.03		± 0.05	± 0.05	± 3.3
			14	2.29	2.35	32.7
				± 0.01	± 0.01	± 0.8
			28	2.27	2.33	37.8
				± 0.04	± 0.04	± 0.2
FD1	1	12.15	7	2.13	2.27	20.4
142		± 0.45		± 0.02	± 0.06	± 1.1
			14	2.17	2.22	22.7
				± 0.01	± 0.01	± 0.4
			28	2.10	2.16	24.6
				± 0.04	± 0.04	± 4.3
FD2	2	10.69	7	2.14	2.19	13.5
141		± 0.46		± 0.01	± 0.01	± 1.2
			14	2.15	2.21	16.9
				± 0.02	± 0.02	± 0.4
			28	2.15	2.22	18.5
				± 0.04	± 0.04	± 2.7
FD3	3	12.25	7	2.22	2.26	18.3
143		± 0.36		± 0.01	± 0.01	± 1.6
			14	2.16	2.21	19.7
				± 0.03	± 0.03	± 5.2
			28	2.16	2.23	22.5
				± 0.02	± 0.02	± 2.3
FDR	raw	11.75	7	2.17	2.21	14.2
144		± 0.84		± 0.01	± 0.01	± 2.7
			14	2.19	2.25	16.7
				± 0.02	± 0.02	± 2.3
			28	2.21	2.28	23.6
				± 0.04	± 0.04	± 1.1

Fig. 2. Main steps of modified mortar formulations using flax residue fillers.

at room temperature under 95 % of relative humidity to ensure uniform conditions across all mixtures. Therefore, the amount of water was the same for all samples. Then, samples are demoulded and stored in water vats. Natural fillers in modified mortars are considered as substitutes. All modified mortars are prepared with a (cement/sand weight ratio of 1:3. The flax residue are added to sand with a fixed weight content of 5 % with respect to the cement (Fig. 2).

3.2. Characterization techniques

The workability of fresh modified mortars is evaluated using flow table tests, following the norms NF EN 1015–3 [43], respectively. The flow test employs a standard conical frustum-shaped mortar with a diameter of 4 in. The mould is cantered on the flow table and filled in two stages with fresh mortar, compacted 15 times during 15 s using a standard-sized temping rod before being lifted vertically from the mould. The percentage change in diameter of the fresh mortar is utilized to calculate flow or consistency evolution.

Before subjecting the modified mortars to mechanical loading, their microstructure is examined. X-ray micro-tomography is employed for

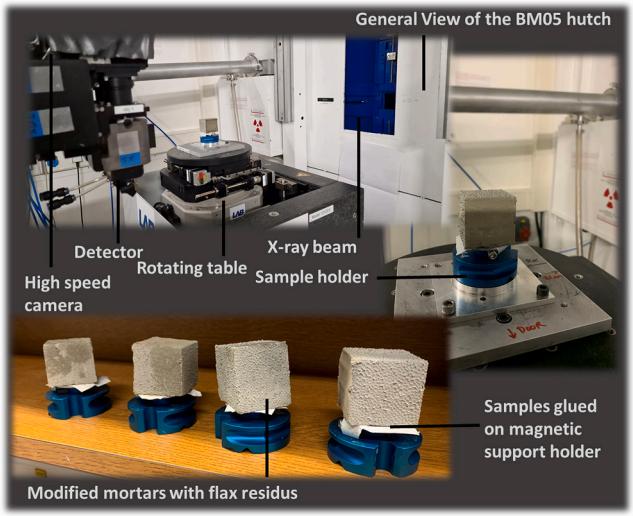

Fig. 3. X-ray μ-tomography characterisation of modified mortars.

three-dimensional imaging of the samples at the ESRF beamline BM5 in Grenoble, France (Fig. 3). The acquisition parameters include a 97 kV energy, a 360° scan range, a 1396 mm working distance, 5000 radiographic images, 101 reference images, 100 dark images, and a detector resolution of 2048 × 2048 pixels. Additionally, a voxel size of 3.04 μm, a count time of 0.015 s, and a latency time of 0.0015 s are set. Reconstruction of the tomograms is accomplished using a back-projection algorithm, with Paganin filtering applied for optimal phase retrieval of phase-contrast images.

To ensure adequate resolution at the specified voxel size, at least three consecutive acquisitions are performed along the height of the sample, effectively doubling the acquired volume. This results in a typical tomogram resolution of 3814 × 3814 × 4200 voxels, covering a cylinder of 11.6 mm in diameter and 12.8 mm in height. Image analysis is conducted using ImageJ software from NIH (USA), which involves various tasks such as brightness calibration, conversion to 256 grey-level images, segmentation, 3D rotation, and filtering using opening and closing operators.

These operations are needed to separate three main phases from the background, namely porosity, flax residues, and cementitious matrix.

Porosity and flax residue contents are measured as the total count of the voxels belonging to each phase as a result of the segmentation.

$$f_{F,T,G,I}(\%) = 100 \times \sum_{i=1}^{N_T} \delta(255 - g_i) \Big/ \sum_{i=1}^{N_T} g_i \tag{1}$$

Wheref_F, f_T, f_G, and f_I are the filler (flax residue), total, spherical and interfacial porosity contents respectively, g_i is the grey level associated with voxel i in the segmented image containing either black ($g_i = 0$) or white ($g_i = 255$) features, N_T is the total number of voxels in the acquired image, δ.is the Kronecker function.

Spherical porosities are separated from the rest of the porosity population using aspect ratio filtering. Their content can be derived as follows

$$f_G(\%) = 100 \times \sum_{i=1}^{N_T} \delta(255 - g_i) \Big/ \sum_{i=1}^{N_T} g_i \quad |\alpha_P > 0.7 \tag{2}$$

Where α_P is the porosity aspect ratio.

Pore connectivity is quantified to determine the proportion of open and close porosities. Open porosity refers to voids that are interconnected and accessible to fluids, while closed porosity consists of isolated voids that do not contribute to permeability. In X-ray microtomography, open pores typically appear as connected networks, with clear paths that extend to the external surface. Closed pores, on the other hand, are seen as isolated, internal voids without direct connections to other pores or the surface. 3D labelling technique is then used to determine the amount of open porosity, which is refereed here as pore connectivity [44]. The pore connectivity is computed as follows

$$C_p(\%) = 100 \times Vm \Big/ \sum_{i=1}^{N_P} V_i \tag{3}$$

Where V_m is the largest connecting pore, V_i is the volume of pore i labelled in 3D based on 6-neighbour connectivity.

Mechanical testing primarily focuses on compressive strength, as it is one of the most important mechanical parameters for assessing mortar performance in structural applications. Bending strength is another essential property that can be evaluated. To conduct this testing, the full space of the 4 × 4 × 16 cm^3 mould is needed to produce standard specimens (Fig. 1), which reduces the number of specimens available for compression testing.

Compression testing is conducted on all samples are performed using 3 R 500 KN machine in accordance with norm ASTM C109 and NF EN: 196–1 [42]. The mechanical characterization is performed on 4 cm cubes at different curing times 7, 14 and 28 days. Load rates recommended by the norm EN: 196–1 are 2400 $N.s^{-1}$ for compression, as per the pre-coded testing protocol. All experiments continue until material rupture occurs. The mechanical resistance referred to as the compression strength is derived for all studied mortars. For each processing condition and curing time, 4 samples are used for compression tests, resulting in a total of 20 mechanical testing trials. The compression strength is derived from compression tests for all formulations.

SEM analysis was conducted on both flax residues and modified mortars to explore how the flax residues affects the compactness of the mortar. Polishing is avoided to prevent the development of cracks and the unintended removal of flax residues from the modified mortars. The investigation utilized a JEOL JSM-5800LV scanning microscope (JEOL-LTD, Tokyo, Japan) operating at an accelerating voltage of 15 kV. For enhanced conductivity during observation, sample surfaces were coated with a 50 nm layer of carbon using a Balzers CED 30 carbon evaporator (OC Oerlikon, Balzers, Liechtenstein). Due to the airiness of the samples, 48 h of storage in ultra-low-pressure environment to remove access of air trapped in the modified mortars. Typical micrographs of 1139 × 912 pixels were acquired. Magnifications were set from 40 × to 4500 ×, with typical pixel sizes ranging from 6 nm to 0.6 μm.

In order to determine the main changes in the composition of flax residues induced by fungal attack, SEM-EDS (Energy-dispersive X-ray spectroscopy) studies were conducted on three types of specimens (Fig. 4): reference flax bundles, fresh and old residues. A scanning microscope JEOL JSM-IT510 (JEOL-LTD, Tokyo, Japan) with integrated EDS, operating at accelerating voltage 15 KV is used. Chemical composition was determined on large regions of interest (1139 × 912 pixels) with typical magnifications were set from 500 × to 200 ×, corresponding to physical dimensions in the range (250 × 190 μm^2 to 630 × 470 μm^2). The probe current is adjusted to 20 nA and spectra acquisition time is fixed to 120 s.

4. Results and discussion

4.1. Microstructure of flax residues

Fig. 4 presents typical micrographs comparing fresh and aged flax residues to a reference flax bundle. The region highlighted in blue indicates the area where elemental analysis was performed. The reference flax micrographs display no evidence of fungal deterioration. In contrast, both fresh and aged residues show surface perforations, with the lateral view of the aged flax residue revealing a hollower structure. Fig. 4b presents the results of EDS materials analysis, highlighting key differences in the presence of certain elements, including Si, K, Cl, and Ca. The spectrum is primarily dominated by oxygen and carbon, reflecting the cellulosic nature of flax. Significant differences are observed in elements such as Ca, K, and particularly Si. To determine whether these variations are related to changes in the fibre composition, EDS was performed on a smaller, debris-free region of interest on the biomass surface. Fig. 5a shows typical micrographs of the analysed regions for all specimens, where voids are observed near the examined area in the old flax residue. Fig. 5b provides a comparative analysis of the EDS spectra. Quantitative estimates of the element content for these small regions are summarized in Table 2. Minor elemental differences, typically below 1 %, are still present. For example, old residues are characterized by the presence of Si, Al, Mg, P, S, and K. The EDS analysis reveals compositional differences between the residues and reference fibres, clearly indicating the impact of a changing environment. However, EDS has limited reliability in assessing the effects of fungal attack. Morphological changes would be a more accurate indicator. SEM micrographs of the reference flax fibres show that the hollow structure seen in the residues is a result of the degradation process.

Fig. 6 SEM micrographs of flax residues shown in Fig. 1 according to the sieving process in Fig. 2. Sampling of the residues is performed to acquire qualitative evaluation of the result of the degradation. Fig. 6a shows a zoom in view on a typical as-received flax residue prior sieving.

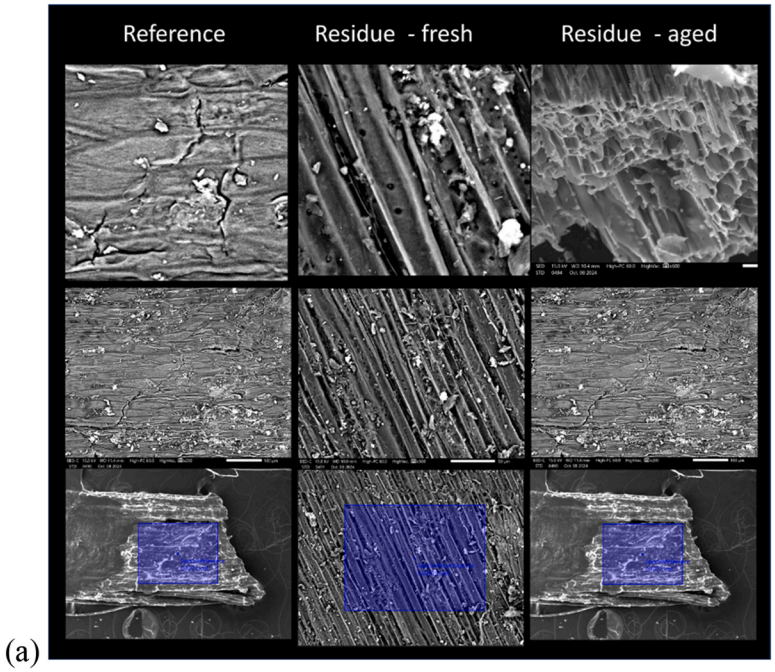

(a)

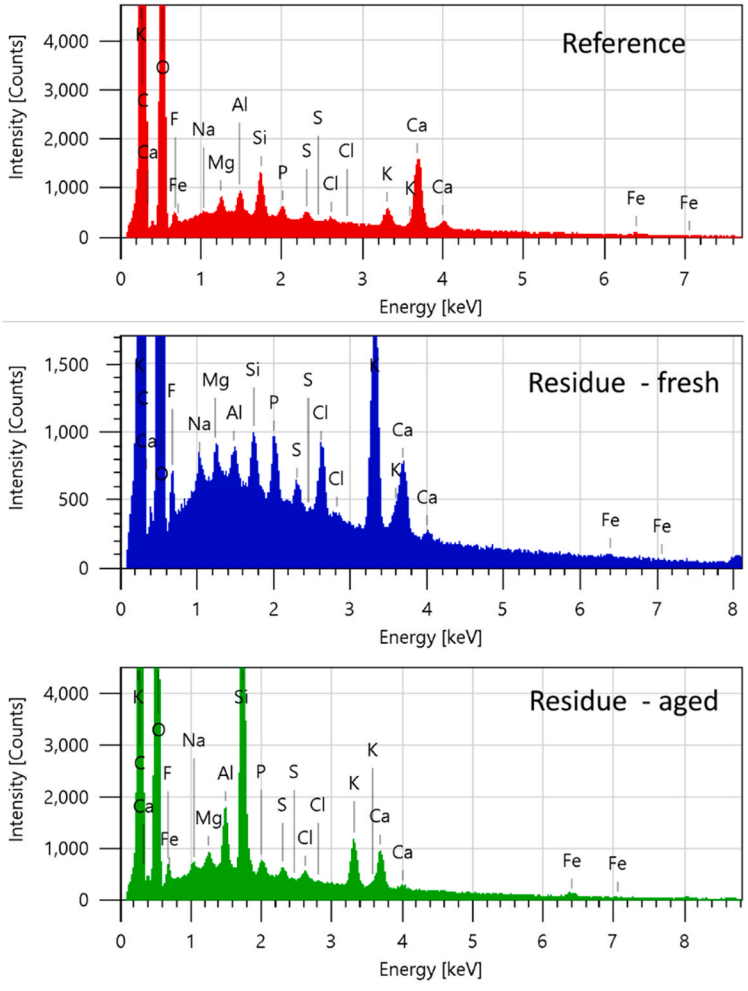

(b)

Fig. 4. SEM-EDS study conducted on reference flax, fresh and aged residues, (a) typical SEM micrographs of the studied samples, (b) EDS Spectrum.

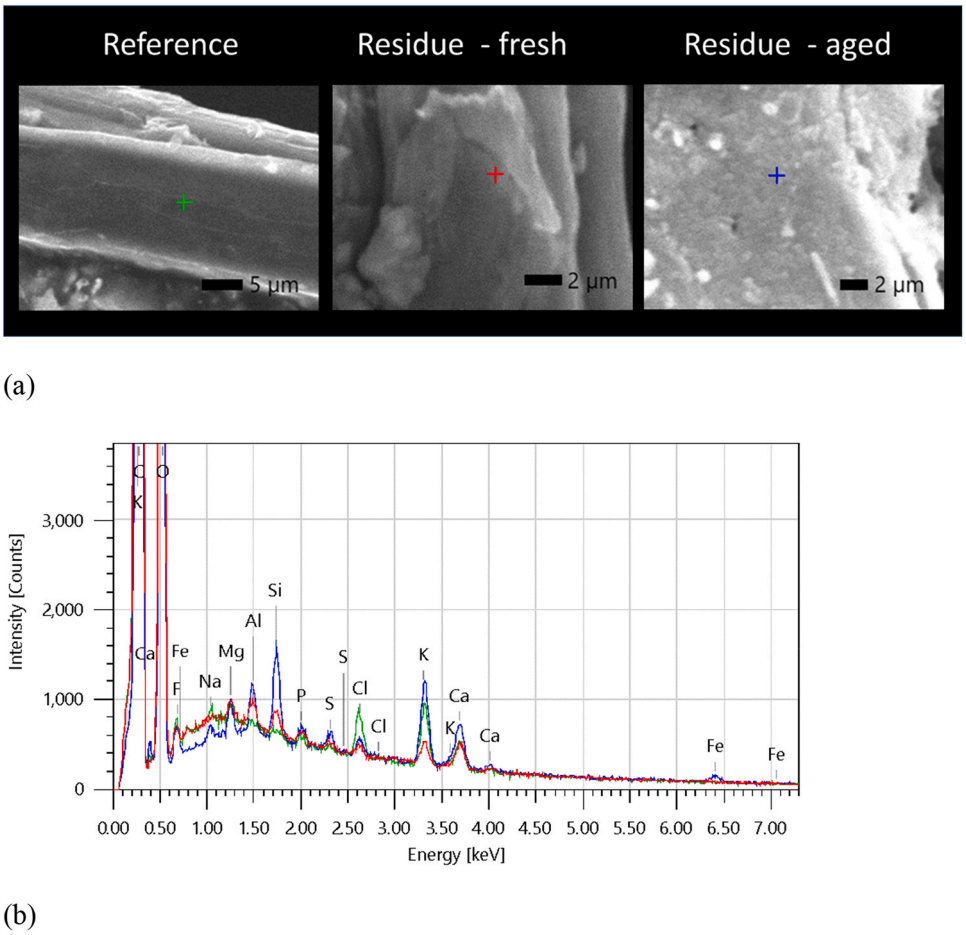

Fig. 5. SEM-EDS study conducted on small region of interest for reference flax, fresh and aged residues, (a) typical SEM micrographs of the studied samples, (b) EDS spectra (green for reference, red for fresh and blue for aged).

Table 2
Elementary analysis performed on large region of interest for reference, fresh and old flax residues.

Element	Reference	Residue - old	Residue - recent
C	72.68	67.5	74.62
O	26.27	28.98	23.82
F	0.35	0.64	0.49
Na	0	0.08	0.06
Mg	0.06	0.16	0.03
Al	0.07	0.22	0.02
Si	0.07	0.43	0.01
P	0.04	0.11	0.03
S	0.03	0.11	0.02
Cl	0.06	0.14	0.25
K	0.15	0.79	0.4
Ca	0.21	0.56	0.25
Fe	0.01	0.27	0
Total	100	100	100

The micrograph shows a hallow structure of a particle of 650 µm in width and at least 1.6 mm in length. Another lateral view reveals an elongated shape where the typical thickness of 60 µm. The aspect ratio representing the ratio between the thickness and the length is close to 0.06. The residue degradation process had led to a significant alteration of the inner tubular structure of the flax residue. This alteration shows clearly the inner lumen space of the unitary cell affected by fungi attack (Fig. 6c). Fungi have the ability to degrade cellulose, hemicellulose, and lignin, which are the primary components of the flax fibres, through the secretion of enzymes like cellulases, hemicellulases, and ligninases. Fungal colonization led to a degradation process shown in Fig. 6c as multiple micrometric porous spots of typical size of 1–3 µm. Fig. 7 show the same particles observed after a sieving process allowing only particles between 2 and 3.15 mm to be selected. The macroscopic view in Fig. 7a shows the contamination of the flax residues left on fields after harvesting, where residues are intertwined with soil particles, particularly during natural decomposition processes. This micrograph also depicts the integration of soil with flax residue such as sand, clay, and organic debris, that adhere to the surface of flax residues. A zoom-in view on the particle cross-section shows a hollow cellular structure with multiple pits corresponding to the more or less irregular enzymic attack leading to a significant airiness of the flax residues. Fig. 7c shows the microstructure of the flax residues, which are subject to further sieving allowing particles of less than 1 mm to be selected. The micrograph shows a particle of about 400 µm in width subject to a combination of enzymatic degradation and mechanical separation processes such as breaking, scutching, and hackling. It is important to note that the density of flax fibres depends on their porosity and water content. As shown in Richely et al.[45], the porosity of flax fibres ranges from 0.4 % to 7 %, which accounts for the typical variation in flax density, usually between 1.4 and 1.5 g/cm^3 . In the case of flax residues, their hollow structure contributes an additional 7–40 % porosity (according to X-ray micro-tomography results), causing the density of flax residues to decrease to a range of 0.84–1.4 g/cm^3 .

4.2. 3D microstructure of modified mortars

Fig. 8a illustrates a comparison between orthogonal perspectives of

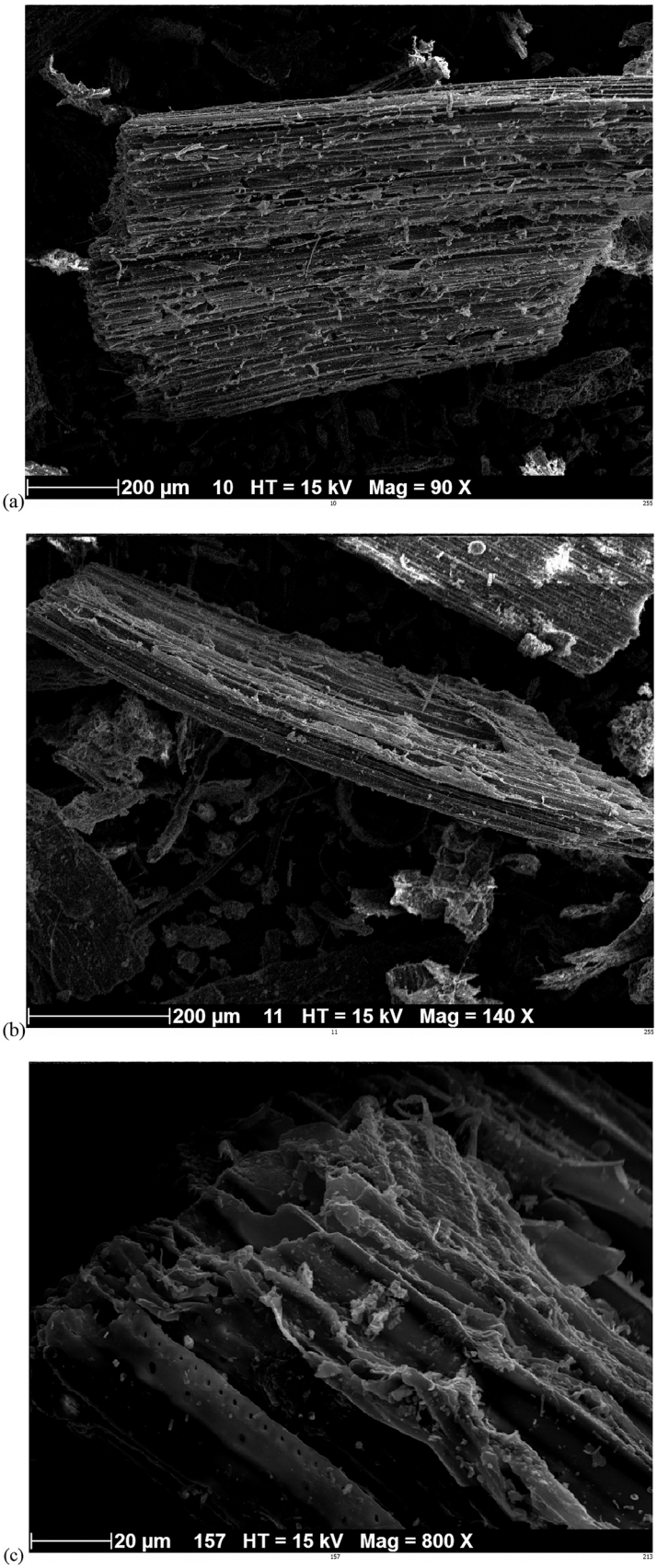

Fig. 6. SEM micrographs detailing the microstructure of flax residues. (a) as-received – zoom-out, (b) zoom-out view normal to the particle section, (c) zoom-in view on the unitary cell.

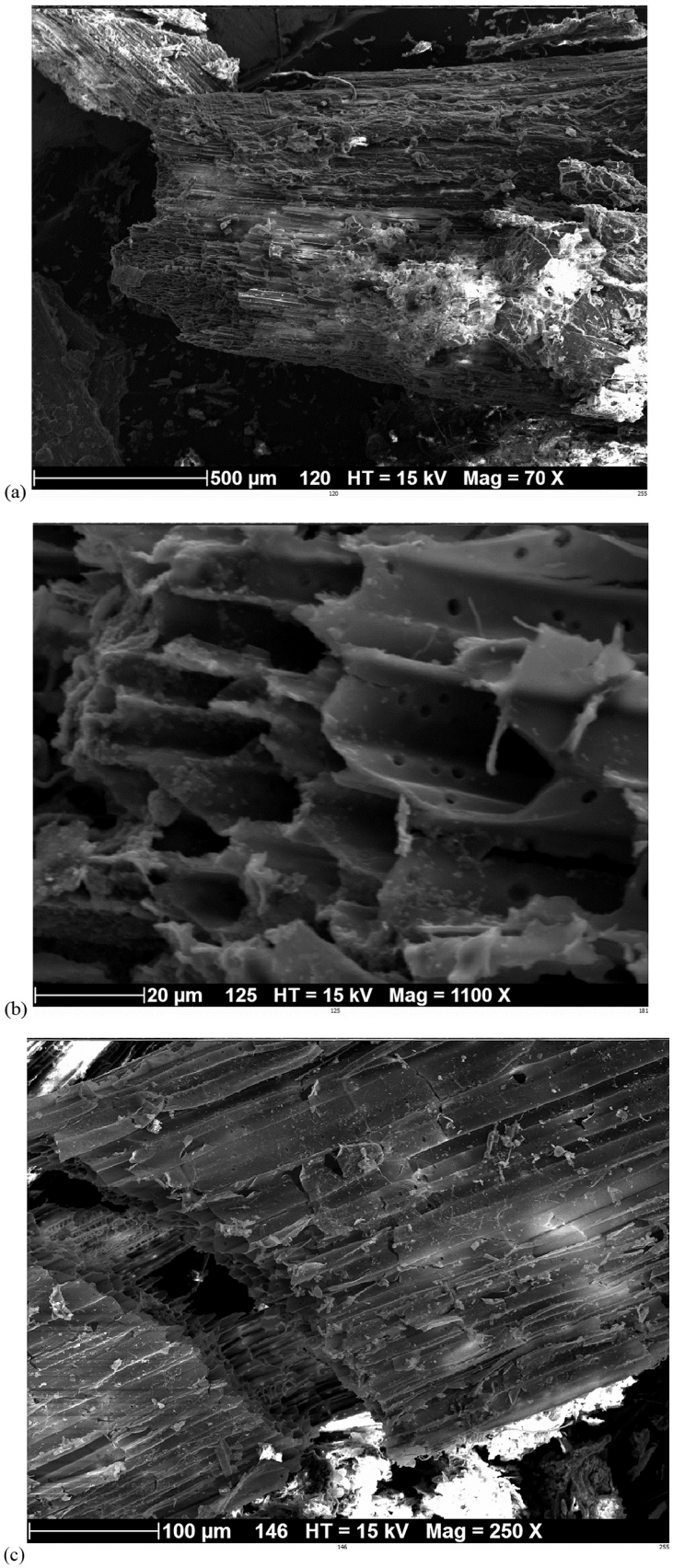

Fig. 7. SEM micrographs detailing the microstructure of flax residues subject to a sieving process. (a) sieving leading to a particle size between 2 and 3.15 mm – zoom-out view (b) Lateral view showing the inner structure of the sieved flax residue. (c) a top view on particles selected after a sieving with the smallest mesh allowing particles below 1 mm to be selected.

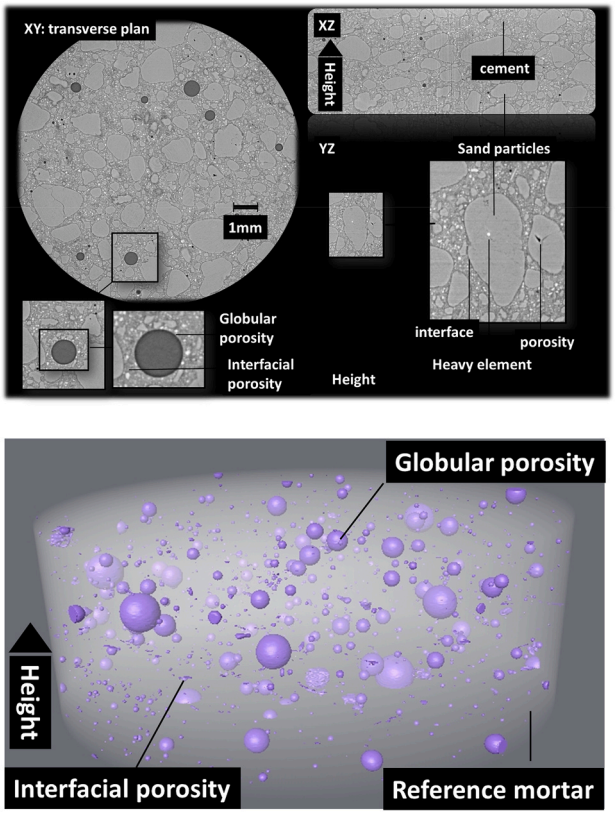

Fig. 8. X-ray microtomography results for reference mortar (a) Orthogonal views underlying the microstructure of reference mortar without flax residues, (b) 3D view of the porous structure.

reference mortar without flax residue addition. These perspectives are generated by combining consecutive tomograms along the specimen's height, with a typical cylindrical in shape Region of Interest of 11.6 mm in diameter and 2 × 4.25 mm in height. In Fig. 8a, the microstructure unveils significant characteristics related to process-induced porosity, a common occurrence in mortar during the mixing stage. The segmentation process effectively distinguishes two types of porosities: large spherical ones induced by air trapped in the cementitious matrix, and smaller ones at the interface between the sand particles and the hydrated cement. All porosities are isolated in the grey level range (1 – 119) by a thresholding process allowing to get rid of the external air as well. In Fig. 8a, the other plans namely XZ and YZ exhibits the same main microstructural features with no particular porous structure anisotropy that might be attributed to the gravity effect during the mixing stage.

Fig. 8b shows the porous structure induced by the formulation of the reference mortar with an overall content below 3 % (Table 3). Based on a particle analysis, which allows separating porosities with respect to their aspect ratio and size, the macroscopic spherical pores representing the trapped air in the mortar represents half of the porosity population. The remaining portion of the population consists of interfacial porosities, which are the spaces between the sand particles and the cementitious matrix. The result of particle analysis, which filters particles of aspect ratio between 0.7 and 1.0 shows that the average content of spherical porosities counts for half of the porosity population associated with the reference mortar.

The XY plane view accentuates key features of typical mortar microstructure, showcasing small number of spherical and macroscopic porosities in the transverse plane associated with the mixing stage. Furthermore, discontinuities close to the sand particles highlight interfacial porosities more or less continuous in the cementitious matrix. Quantification of the porosity contents are outlined in Table 3 for the reference material. It features a small amount of porosity, mainly triggered by the population of sand particles.

Fig. 9a shows the same X-ray microtomography cross-sections of a modified mortar with flax residues of a typical size of 2 mm. Besides the porosity depicted in all planes, there is a clear distinction between the cementitious matrix and the natural filler because of the difference in phase morphology. However, these residues appear as a dark grey level overlapping more or less with the porosity grey level. It has to be mentioned that porosity content does not seem to be much affected by the presence of the flax residues. In addition, these residues are homogeneously distributed in the cementitious matrix. Despite the elongated shape of the flax residues, the 3D microstructural characterization does not show particles larger than 2 mm.

The spatial distribution of both process-induced porosity and flax residues do not display regular patterns with discernible preferred

Table 3
Microstructure results for all studied modified mortars:: f_F Flax residue content; f_T Total porosity content; f_G: spherical porosity content; f_I: Interfacial porosity content; C_p(%): pore connectivity (open porosity).

Sample	f_F (%)	f_T (%)	f_G (%)	f_I (%)	C_p(%)
FD0	-	2.78 ± 0.16	1.46 ± 0.11	1.32 ± 0.27	7.22 ± 2.61
FD1	3.83 ± 1.33	2.89 ± 0.88	2.14 ± 0.46	0.74 ± 0.41	12.25 ± 2.60
FD2	6.06 ± 0.20	4.18 ± 0.51	2.59 ± 0.32	1.59 ± 0.20	35.17 ± 27.10
FD3	5.30 ± 0.19	4.31 ± 0.07	2.00 ± 0.08	2.31 ± 0.01	10.31 ± 4.95
FDR	5.36 ± 2.18	8.83 ± 0.22	2.70 ± 0.32	6.07 ± 0.20	17.98 ± 4.52

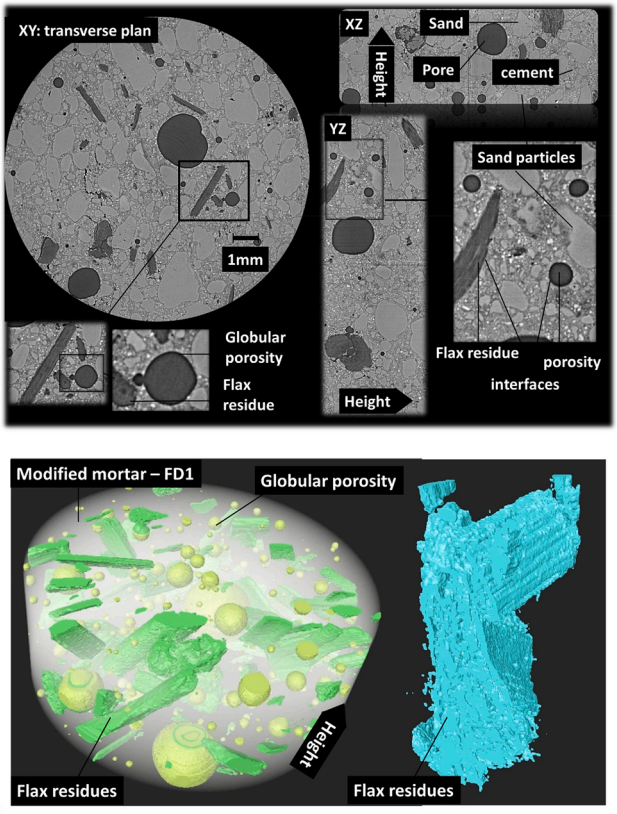

Fig. 9. X-ray microtomography results for modified mortars with flax residues as large as 2 mm – samples FD1 (a) Orthogonal views underlying the microstructure of modified mortar with flax residues, (b) 3D view of the porous structure and flax residues imbedded in the cementitious matrix.

orientations. The segmentation process reveals the same two main types of porosities: large spherical porosities associated with the air trapped inside the mortar and micro-porosity associated to the lack of adhesion between cement and the other phases including the flax residues and sand.

Fig. 10a presents analogous orthogonal perspectives of various formulations for different flax residue sizes. The figure emphasizes the distinctive arrangements of flax residues, where FDR includes both large and small residues, while FD1 contains only small flax particles. Positioned between these two formulations, FD3 displays more regular and larger flax residues within the mortar matrix.

Similar macroscopic and microscopic porosities are observed for all formulation, and discerning their magnitude in comparison to sample FD2 is not immediately apparent. Similar to the previous case, process-

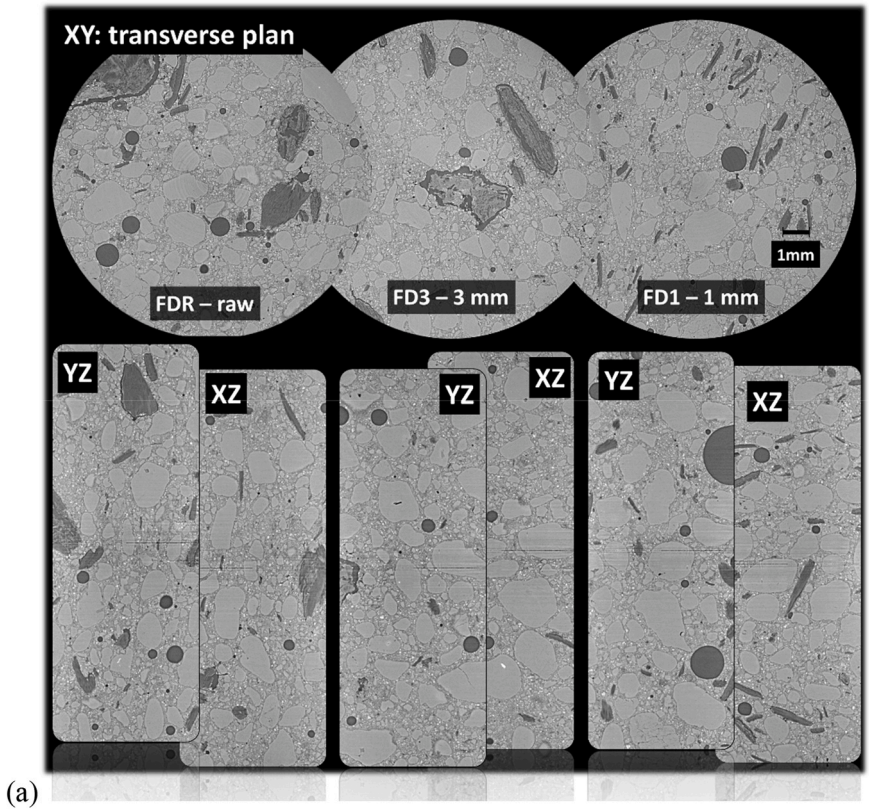

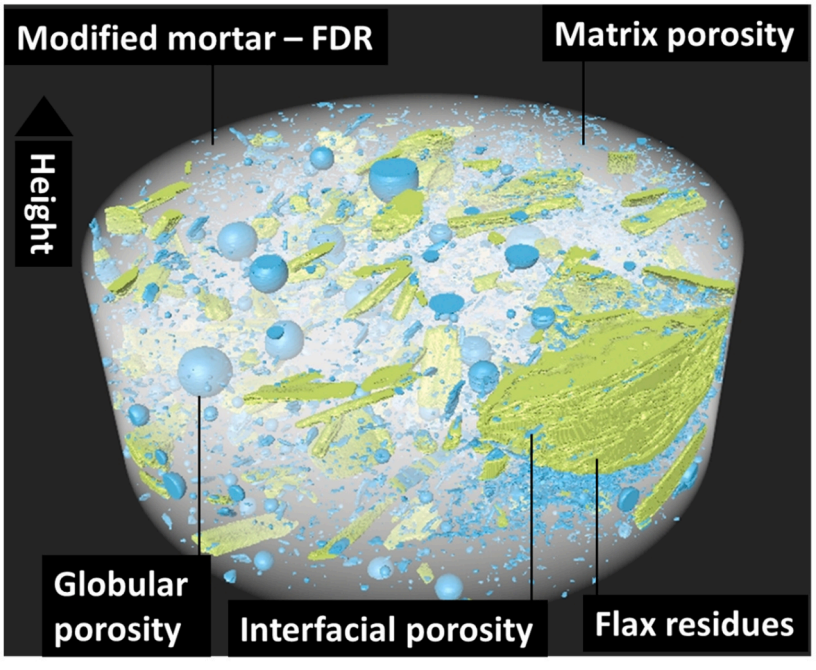

Fig. 10. X-ray microtomography results for modified mortars with different flax residue diameters. (a) Orthogonal views underlying the microstructure of reference mortar without flax residues, (b) 3D view of the porous structure and flax residues imbedded in the cementitious matrix for sample FDR.

induced porosity does not compromise the cohesion of the mortar with the flax residues. This is more the case for formulations containing large residues such as FD3 or FDR, where a clear discontinuity between the flax particles and the matrix is observed.

The resulting segmented phases are further exploited in Fig. 10b. This figure presents perspective views of the porous structures for all formulations. The overall porous structure resembles that of sample FD1 (Fig. 9), but with a greater prevalence of interfacial porosities. Additionally, two other types of porosities are identified in all formulations such as in FDR (Fig. 10b): porosities within the matrix and within the residues themselves. These porosities merge with each other allowing a significant connectivity to take place.

Table 3 provides a quantitative evaluation of the porosity and filler content trends. Despite the rigorous protocol observed in the preparation of the samples, there is still a variability in the flax residue contents. Indeed, the extracted contents from image analysis shows a wide range from 4 % to 6 % against a theoretical content of 5 %. This variability can be explained by the representativity of the region of interest imaged compared to the overall formulated samples. The analysis of the total porosity contents shows two main findings. The modified mortar with raw flax residues, which are not sieved, trigger the largest porosity content. The best formulation seems to be the one formulated with 1 mm flax residues. This result indicates that fine flax particles have the lowest effect on porosity development during the mixing stage. The porosity trend is found to depend on the type of porosity. Spherical porosities do not follow any particular trend. Their content seems to be stable around 2 %. However, significant change in the interfacial porosity is found depending on the formulations. Indeed, most of the change of the total porosity is explained by the sensitivity of the interfacial porosity to the flax residue seining.

The differentiation between open and closed porosities in modified mortars is based on pore connectivity. Fig. 11 illustrates the types of pore connectivity identified using 3D labelling techniques. In the reference condition, the connectivity is generally low, with most cases showing two or three adjacent pores that share common surfaces. As shown in Table 3, the pore connectivity typically does not exceed 10 %. Sample FD1, containing flax residues up to 1 mm in size, exhibits higher connectivity (Table 3). This increased connectivity is explained by the merging of larger pores and the presence of smaller, satellite pores linked to the larger ones, as shown in Fig. 11. Additionally, pore-flax residue connectivity is prominent, further enhancing connectivity due to the hollow structure of the flax residues. It is important to note that this connectivity involving the solid phase is not included in the connectivity count presented in Table 3. For sample FD2, a significant discrepancy is observed in the connectivity results, which is reflected by the large standard deviation (Table 3). The overall trend still demonstrates that the connectivity increases alongside the rise in porosity content for all modified mortars.

4.3. Workability of modified mortars

The effect of natural fibres on mortar flowability is debated. Depending on fibre size and water content, flowability can either improve or deteriorate [46–48]. As shown by the workability results in Table 1, flax residues delay mortar flow. The correlation between the flax residue size ϕ and the flow of modified mortar expressed as the percentage of the increase in mould diameter ω suggests an exponential trend. This relationship can be quantified using the following empirical expressions, including the correlation factor (R^2). This suggests

$$\omega(\%) \approx 11.52 + 4.54 \times \exp(-\phi(mm)/0.44); R^2 = 0.92 \quad (4)$$

Where ϕ varies between 1 and 3 mm. It is worth mentioning that the formulation FDR is excluded from the analysis.

Workability investigation using flow table experiments suggests more steady mortars modified with flax residues below 1 mm in size. Lack of fluidity is unexpectedly not observed for FD3 formulation. Fig. 1 provides an explanation from the shape factor of the residues, where more spherical particles are present than elongated ones. It has to be mentioned that the variations observed in workability are not due to differences in water content rather to the presence of flax residues, which limit flowability of modified mortars depending on the content and morphology.

4.4. Mechanical performance of modified mortars

Table 1 presents the results of mechanical testing as a function of curing days for all the formulations tested. None of the formulations outperformed the reference mortar. The formulations that came closest to the reference performance were FD1 and FD3, corresponding to the largest $\phi =$ mm) and smallest ($\phi =$ mm) residue sizes.

An increase in compressive strength (σ_C) is observed with longer curing times. However, the trend related to residue size remains unclear. The results indicate that small flax residues or large spherical ones have a beneficial effect. The mechanical strength loss is 26 % for FD1 and 34 % for FD3. The other formulations show more varied effects on compression performance, making it difficult to determine a clear tendency regarding flax residue size. When considering the longest curing time as a reference for the best performance, FD1 shows a 35 % loss in compression strength, the lowest among all formulations. This suggests that mortars modified with small residues combine good workability and compression performance.

Fig. 12 displays differences in rupture modes through optical micrographs showing the cracking patterns as a function of curing time for all studied formulations. All samples exhibit brittle rupture with crack branching, likely dominated by a prevailing opening mode. The compression response suggests a more gradual damage evolution for

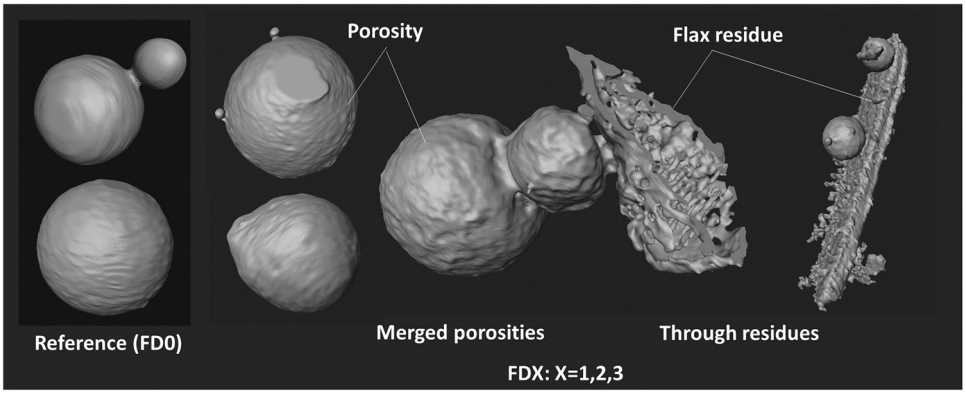

Fig. 11. Pore connectivity as a function of flax residue content.

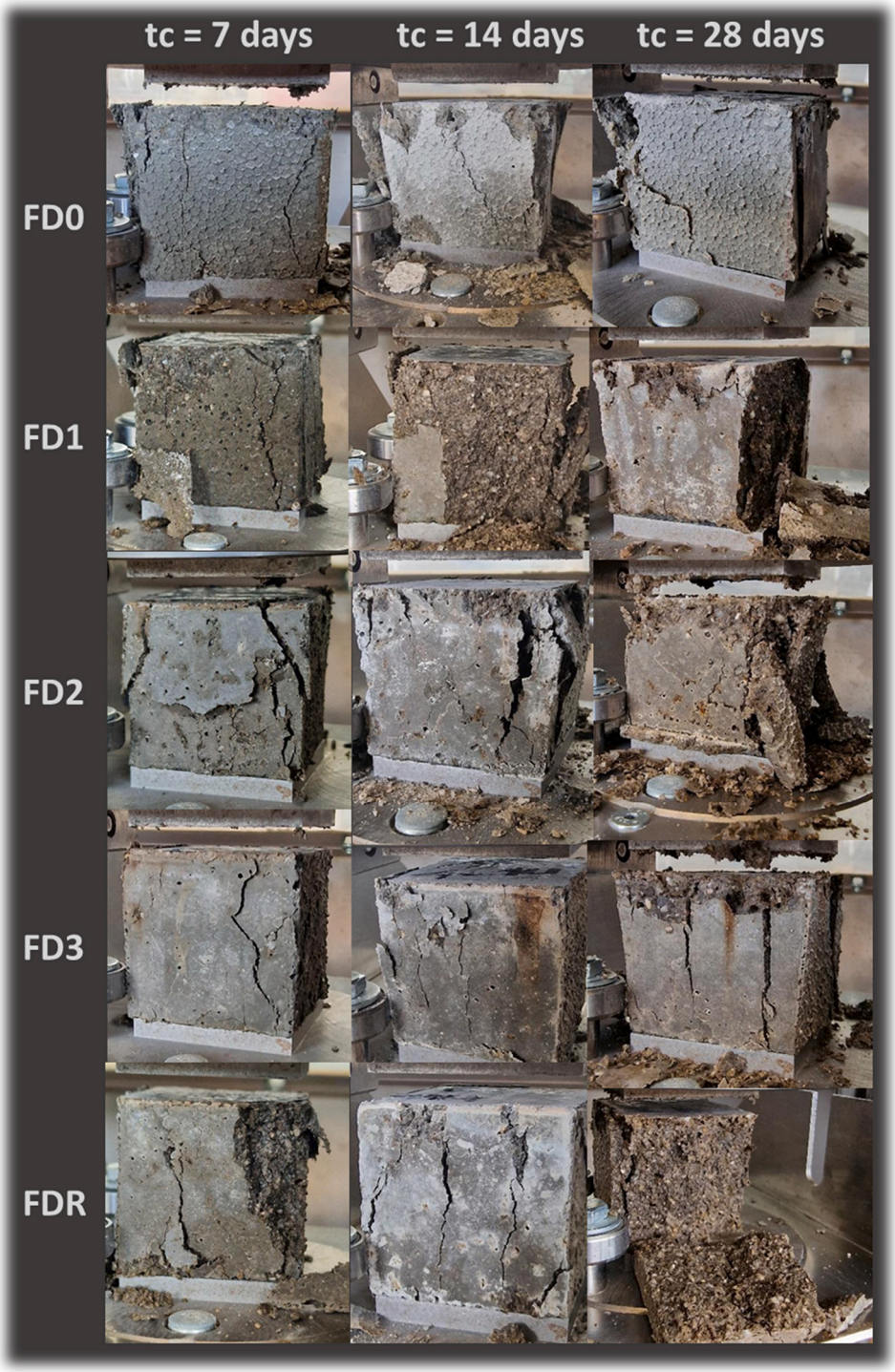

Fig. 12. Rupture patterns upon compression of modified mortars as a function of size of flax residues and curing time.

samples containing flax residues, which prevents complete failure of the modified mortars, as seen in FD3. Some formulations show cracking that leads to partial or complete separation of large parts of the sample, evident in FD1 and FDR, where interfacial porosities likely play a significant role in generating such cracking patterns.

For other formulations, the addition of flax residues delays the rupture of mortar under compressive load, associated with larger ultimate deformation. An overall analysis of the compression results in Table 1 suggests a linear increase in mechanical strength (σ_C) with curing time. These profiles are influenced by the size of the flax residues. Assuming secondary cross effects, the linear fitting produces the following correlations:

For FD0:

$$\sigma_C(MPa) = 27 + 0.38 \times t_C(days); R^2 = 0.99 \quad (5)$$

The same fitting result reads for the modified mortars

$$\sigma_{C\_FD1}(MPa) = 18.68 + 0.28 \times t_C(days); R^2 = 0.93 \quad (6)$$

$$\sigma_{C\_FD2}(MPa) = 12.34 + 0.31 \times t_C(days); R^2 = 0.93 \quad (7)$$

$$\sigma_{C\_FD3}(MPa) = 16.90 + 0.20 \times t_C(days); R^2 = 1.00 \quad (8)$$

$$\sigma_{C\_FDR}(MPa) = 10.60 + 0.46 \times t_C(days); R^2 = 0.99 \quad (9)$$

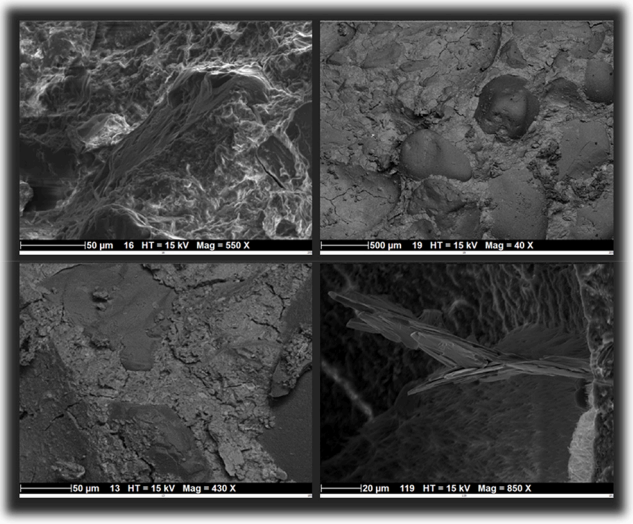

(a)

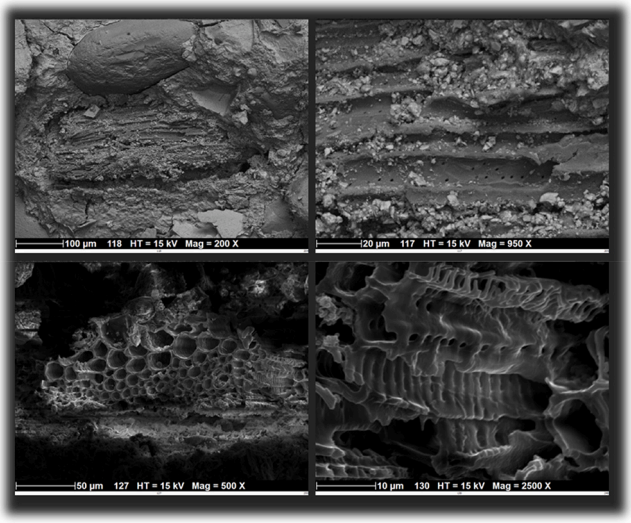

(b)

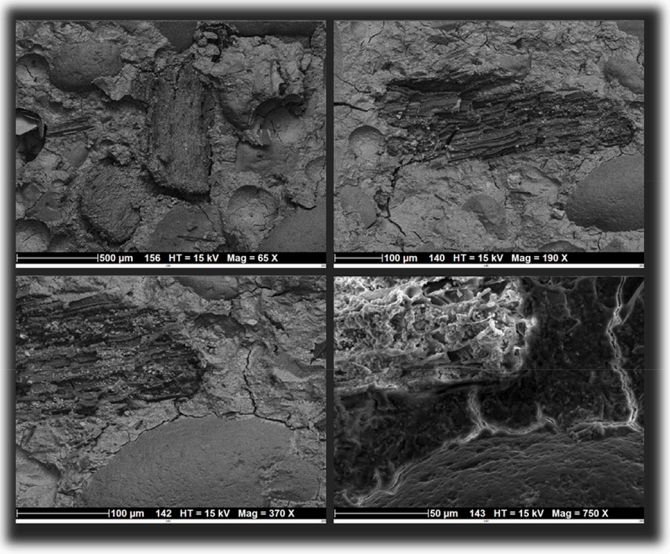

(c)

Fig. 13. SEM micrographs of ruptured samples. (a) FD0, (b) FD1, (c) FD2, (c) FD3, (d) FDR.

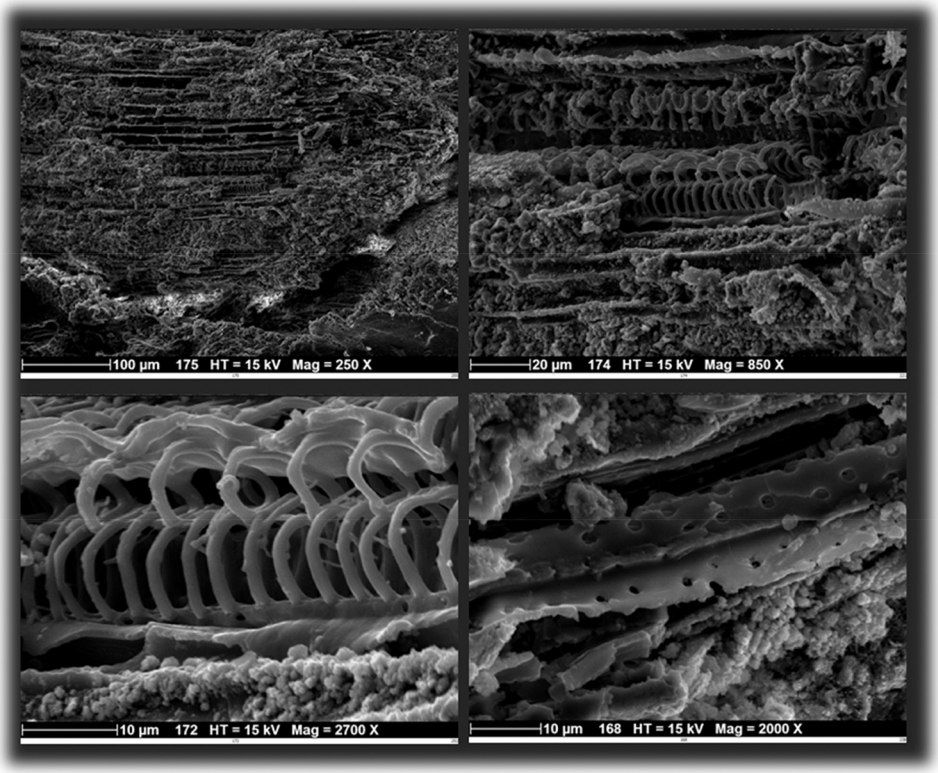

(d)

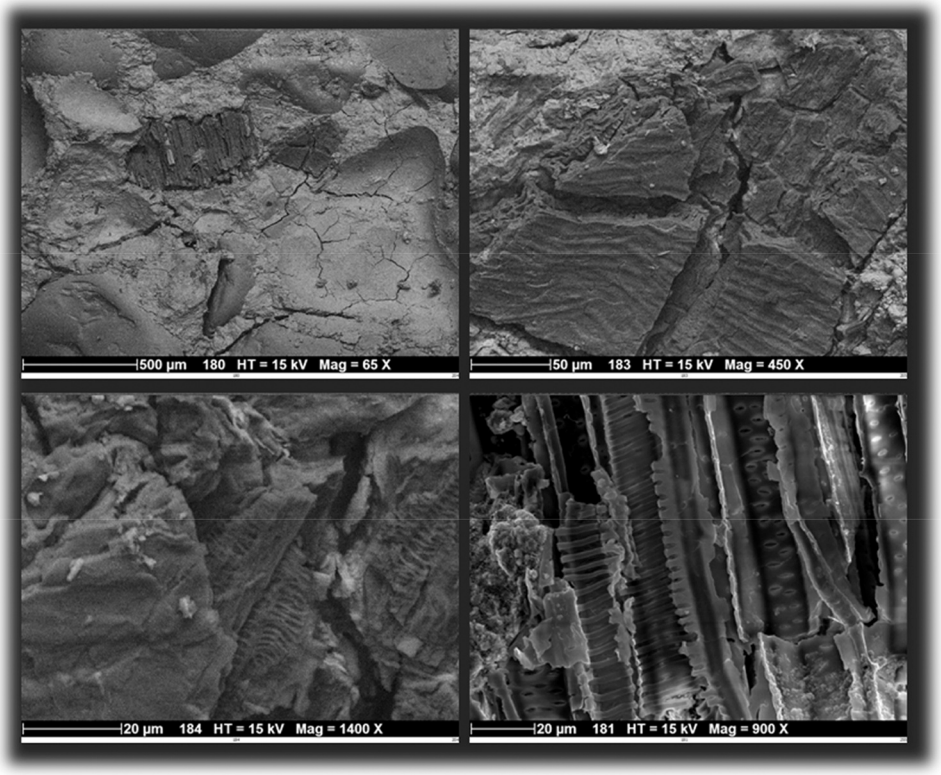

(f)

Fig. 13. (*continued*).

Where σ_{C_FD1}, σ_{C_FD2}, σ_{C_FD3} and σ_{C_FDR} refers to the compression strength of modified mortars FD1, FD2, FD3, and FDR, respectively.

4.5. SEM evidence of flax residue effect on modified mortar performance

SEM analysis of ruptured samples allows to gain insights into the impact of flax residues on the microstructural properties and performance of the modified mortars. Fig. 13a depicts SEM micrographs of a reference mortar without the addition of flax residues. The SEM reveal a dense and relatively uniform microstructure. The matrix appears compact, with well-defined hydration products such as calcium silicate hydrates (CSH) and portlandite plates. The absence of flax residues contributes to a homogenous distribution of these hydration phases, leading to a consistent and smooth surface texture. The pore structure is predominantly fine and evenly distributed, indicative of efficient packing and good workability. Minimal microcracks are observed, suggesting that the reference mortar possesses good intrinsic mechanical properties. Overall, the micrographs in Fig. 13a depict a mortar matrix with a low porosity and high density, characteristics that are typically associated with strong and durable cementitious materials. This baseline structural integrity provides a clear contrast when compared to the more complex microstructure of flax residues-modified mortars as shown in Fig. 13b. The micrographs associated with the FD1 formulation highlights the impact of small flax residues on the mortar's overall morphology and performance characteristics. There is a relatively uniform distribution of flax residues throughout the matrix, indicating effective mixing. The residue-matrix interface appears well-bonded, with minimal signs of debonding, suggesting good stress transfer between the residues and the matrix. The residues themselves are largely intact, showing no significant signs of damage or degradation, except the one occurred before the mixing stage. The airiness of the residues is also preserved during the mechanical mixing, which implies a good compatibility with the mortar's chemical and physical environment.

Fig. 13c shows the same micrographs for modified mortars with larger flax residues. Besides the same microstructural arrangements, some clustering of the residues is observed, which could potentially create weak points in the structure. The cracking pattern seems to involve both microcracks from the cementitious matrix which connects to the flax residue/sand interfaces. Overall, the formulation FD2 displays a more tortuous microstructure with crack-bridging capabilities. This crack-bridging could be a leverage to improve the durability by delaying instable cracking. However, the clustering of flax residues and the interfacial porosities identified from X-ray micro-tomography run against delaying mechanical instability.

Fig. 13d shows the microstructure features of one of the best performing formulation, namely FD3. Flax residues seem strongly bonded to the cementitious matrix. These also appear in their initial airy state. In addition, the cement effectively infiltrates the airy flax residues, enhancing the composite's structural integrity by filling voids and creating a denser, more cohesive matrix.

Fig. 13f shows the cracking patterns and microstructural features of the mortar formulation obtained with the as-received flax residue. The micrographs show evidence of inter-residue cracking and damage, which can be attributed to a large load transfer to the filler. In addition, the filler morphology seems to be altered as the inner part of the tubular morphology of flax is further exposed.

5. Discussion of main effects

From the SEM evidence, the hollow structure of the flax residue attests on advanced stage of biodegradation. Indeed, the biodegradation is defined as a process in which enzymes from microorganisms—such as bacteria, fungi, actinomycetes, and algae—cause chemical changes [49]. Natural fibres degrade first into simple elements, and glucose is disintegrated into carbon dioxide and methane gases [50]. Most of the available literature on natural filler biodegradability is related to the study of degradability of biobased composites. For instance, Muniyasamy et al. [51], investigated the biodegradation of flax fiber–PHBV composites, presenting SEM evidence of microbial degradation, including the presence of fungal mycelia on the composite surface. Similarly, Crawford et al. [52] examined the impact of fungal deterioration on the mechanical properties of flax fiber-reinforced composites. Their study revealed a 43 % reduction in stiffness and demonstrated, through weight loss monitoring, the consumption of natural material due to fungal activity.

The microstructure of modified mortars shows porosity resulting from the addition of fillers in the cementitious matrix. Ajouguim et al. [53] investigated how incorporating alfa plant fibres affects the mechanical properties of cement mortars. Their findings revealed a correlation between fibre content and porosity level, which ranged from 8 % to nearly 20 %.

The reduction in workability of modified mortars due to the addition of flax residues aligns with findings from various studies. For example, Wongsa et al. [54] examined the flow of natural fibre-reinforced high-calcium fly ash geopolymer mortar. They observed a significant linear decrease in workability, dropping from 100 % to 20 %, as fibre content increased within the 0.5 %–1 % range. Other studies assess the impact of fibre reinforcement based on fibre type. For instance, Kurpińska et al. [55] showed that the fluidity of modified mortars with natural fibres improved with bamboo fibres, decreased with ramie and cotton fibres, and was nearly unaffected by sisal fibres.

Our results on the mechanical performance of modified mortars clearly indicate that small residues achieve a good balance between workability and compressive strength. The reduction in performance due to natural fillers is well documented in the literature. For instance, de Oliveira Libório Dourado et al. [56] found that adding babassu fibres to mortar reduced compressive strength. This decrease was primarily driven by porosity levels, which peaked at 1.8 % fibre content by weight, resulting in approximately 18 % porosity in the modified mortar. Similar results were achieved by Kurpińska et al.[55] for a variety of natural fibres where the compressive strength is affected in a wide range from −4 % down to −27 % depending on the fibre type.

6. Conclusions

This study thoroughly investigated the effect of flax residues on the microstructural and mechanical properties of cementitious materials, emphasizing key aspects such as porosity, workability, and overall performance. The findings demonstrate that the size and content of flax residues significantly influence the optimization of mortar properties, paving the way for more sustainable and efficient construction materials. The key conclusions are as follows.

- The inclusion of flax residues in cementitious materials demonstrated a measurable influence on porosity. Finer flax residues, particularly those under 1 mm in size, exhibited a minimal impact on overall porosity (<3 %), suggesting that flax residue size plays a pivotal role in optimizing the microstructure. In contrast, larger particles (>2 mm) introduced more significant porosity, potentially compromising structural integrity of modified mortars.
- The workability assessments revealed that the introduction of flax residues delays mortar flow, with an exponential correlation between residue size and the degree of flow reduction. Specifically, larger flax particles were found to increase internal friction, leading to a more pronounced decline in workability. This highlights the complexity of maintaining an optimal balance between mechanical performance and fluidity in the flax residue - mortar formulations.
- The incorporation of flax residues, particularly after a sieving process, allowed the achievement of compressive strengths as high as 20 MPa after just 7 days of curing. This demonstrates that flax

residues can serve as a viable eco-friendly additive, provided that particle size and content are rigorously controlled.

- Achieving a balance between enhanced mechanical properties and workability remains a key challenge. The findings indicate that flax residue content up to 5 % can modify both the functional and structural properties of mortars. Future research should focus on optimizing residue content and size distribution. Additionally, introducing a third reinforcing phase with superior mechanical properties may further improve the strength and durability of flax-reinforced mortars.

CRediT authorship contribution statement

Sofiane Guessasma: Writing – original draft, Visualization, Validation, Supervision, Resources, Project administration, Methodology, Investigation, Formal analysis, Data curation, Conceptualization. **Nicolas Stephant:** Writing – review & editing, Visualization, Software, Methodology, Investigation, Formal analysis, Data curation. **Lotfi Hedjazi:** Writing – review & editing, Supervision, Resources, Methodology, Investigation, Formal analysis, Data curation, Conceptualization.

Declaration of Competing Interest

The authors declare that they have no known competing financial interests or personal relationships that could have appeared to influence the work reported in this paper.

Data availability

Data will be made available on request.

References

[1] F. Pacheco-Torgal, S. Jalali, Cementitious building materials reinforced with vegetable fibres: a review, Constr. Build. Mater. 25 (2011) 575–581.
[2] O.S. Abiola, W.K. Kupolati, E.R. Sadiku, J.M. Ndambuki, Utilisation of natural fibre as modifier in bituminous mixes: a review, Constr. Build. Mater. 54 (2014) 305–312.
[3] R.S.P. Coutts, A review of Australian research into natural fibre cement composites, Cem. Concr. Compos. 27 (2005) 518–526.
[4] M.K. Madhavan, D. Sathyan, K. Jayanarayanan, Hybrid natural fiber composites in civil engineering applications, Hybrid. Nat. Fiber Compos. (2021) 41–72.
[5] N. Trochoutsou, M. Di Benedetti, K. Pilakoutas, M. Guadagnini, Mechanical characterisation of flax and jute textile-reinforced mortars, Constr. Build. Mater. 271 (2021).
[6] T. Hirano, S. Kato, S. Murakami, T. Ikaga, Y. Shiraishi, H. Uehara, A study on a porous residential building model in hot and humid regions part 2 - reducing the cooling load by component-scale voids and the CO2 emission reduction effect of the building model, Build. Environ. 41 (2006) 33–44.
[7] P. Dräger, P. Letmathe, Value losses and environmental impacts in the construction industry – tradeoffs or correlates? J. Clean. Prod. 336 (2022).
[8] L. Gustavsson, A. Joelsson, R. Sathre, Life cycle primary energy use and carbon emission of an eight-storey wood-framed apartment building, Energy Build. 42 (2010) 230–242.
[9] B. Dams, D. Maskell, A. Shea, S. Allen, V. Cascione, P. Walker, Upscaling bio-based construction: challenges and opportunities, Build. Res. Inf. 51 (2023) 764–782.
[10] J. Nassen, J. Holmberg, A. Wadeskog, M. Nyman, Direct and indirect energy use and carbon emissions in the production phase of buildings: an input-output analysis, Energy 32 (2007) 1593–1602.
[11] F.F. Fu, H.B. Luo, H. Zhong, A. Hill, Development of a carbon emission calculations system for optimizing building plan based on the LCA framework, Math. Probl. Eng. (2014).
[12] E. Georgopoulou, Y. Sarafidis, S. Mirasgedis, C.A. Balaras, A. Gaglia, D.P. Lalas, Evaluating the need for economic support policies in promoting greenhouse gas emission reduction measures in the building sector: the case of Greece, Energy Policy 34 (2006) 2012–2031.
[13] X.Z. Gong, Z.R. Nie, Z.H. Wang, S.P. Cui, F. Gao, T.Y. Zuo, Life cycle energy consumption and carbon dioxide emission of residential building designs in beijing a comparative study, J. Ind. Ecol. 16 (2012) 576–587.
[14] C. Ji, T. Hong, H.S. Park, Comparative analysis of decision-making methods for integrating cost and CO2 emission - focus on building structural design, Energ. Build. 72 (2014) 186–194.
[15] F. Khan, N. Hossain, F. Hasan, S.M.M. Rahman, S. Khan, A.Z.A. Saifullah, M. A. Chowdhury, Advances of natural fiber composites in diverse engineering applications—a review, Appl. Eng. Sci. 18 (2024).
[16] E. Richely, A. Bourmaud, V. Placet, S. Guessasma, J. Beaugrand, A critical review of the ultrastructure, mechanics and modelling of flax fibres and their defects, Prog. Mater. Sci. (2021) 100851.
[17] H.L. Luo, G.Y. Xiong, C.Y. Ma, D.Y. Li, Y.Z. Wan, Preparation and performance of long carbon fiber reinforced polyamide 6 composites injection-molded from core/shell structured pellets, Mater. Des. 64 (2014) 294–300.
[18] S. Elfordy, F. Lucas, F. Tancret, Y. Scudeller, L. Goudet, Mechanical and thermal properties of lime and hemp concrete ("hempcrete") manufactured by a projection process, Constr. Build. Mater. 22 (2008) 2116–2123.
[19] L. Arnaud, E. Gourlay, Experimental study of parameters influencing mechanical properties of hemp concretes, Constr. Build. Mater. 28 (2012) 50–56.
[20] O. Homoro, S. Amziane, M.C. Canullo, R. Contamine, Mechanical characterization of flax textile reinforced cement matrix: effect of matrix parameters and reinforcement amount, Eur. J. Environ. Civ. Eng. 27 (2023) 4528–4543.
[21] P. Basu, R. Kumar, M. Das, Natural and manmade fibers as sustainable building materials, Mater. Today Proc. (2023).
[22] N. Kouta, J. Saliba, N. Saiyouri, Fracture behavior of flax fibers reinforced earth concrete, Eng. Fract. Mech. 241 (2021).
[23] S. Niyasom, N. Tangboriboon, Development of biomaterial fillers using eggshells, water hyacinth fibers, and banana fibers for green concrete construction, Constr. Build. Mater. 283 (2021) 122627.
[24] M.T. Marvila, J. Alexandre, A.R.G. de Azevedo, E.B. Zanelato, Evaluation of the use of marble waste in hydrated lime cement mortar based, J. Mater. Cycles Waste Manag. 21 (2019) 1250–1261.
[25] M.E.A. Fidelis, R.D. Toledo Filho, F. de Andrade Silva, B. Mobasher, S. Müller, V. Mechtcherine, Interface characteristics of jute fiber systems in a cementitious matrix, Cem. Concr. Res. 116 (2019) 252–265.
[26] M.A. Mosaberpanah, S.B. Olabimtan, A.P. Balkis, B.O. Rabiu, B.O. Oluwole, C. S. Ajuonuma, Effect of biochar and sewage sludge ash as partial replacement for cement in cementitious composites: mechanical, and durability properties, Sustainability 16 (2024) 1522.
[27] L. Ghalieh, E. Awwad, G. Saad, H. Khatib, M. Mabsout, Concrete columns wrapped with hemp fiber reinforced polymer – an experimental study, Procedia Eng. 200 (2017) 440–447.
[28] R. Prakash, S.N. Raman, N. Divyah, C. Subramanian, C. Vijayaprabha, S. Praveenkumar, Fresh and mechanical characteristics of roselle fibre reinforced self-compacting concrete incorporating fly ash and metakaolin, Constr. Build. Mater. 290 (2021) 123209.
[29] G. Ferrara, M. Pepe, E. Martinelli, R.D. Tolêdo Filho, Tensile behavior of flax textile reinforced lime-mortar: influence of reinforcement amount and textile impregnation, Cem. Concr. Compos. 119 (2021).
[30] M.Z. Rahman, Mechanical and damping performances of flax fibre composites – a review, Compos. Part C Open Access 4 (2021).
[31] L. Yan, N. Chouw, K. Jayaraman, Flax fibre and its composites – a review, Compos. Part B Eng. 56 (2014) 296–317.
[32] A.B. Thomsen, S. Rasmussen, V. Bohn, K. Vad Nielsen, A. Thygesen, Hemp raw materials: The effect ofcultivar, growth conditions and pretreatment on the chemical composition of the fibres, Risø Natio Laboratory Report, Denmark, 2005.
[33] C. Morvan, C. Andème-Onzighi, R. Girault, D.S. Himmelsbach, A. Driouich, D. E. Akin, Building flax fibres: more than one brick in the walls, Plant Physiol. Biochem. 41 (2003) 935–944.
[34] B.S. Panigrahy, J. Fung, S. Panigrahi, A. Tripathy, B. Rajakumar, A. Kamal, Flax fibre based composite profiles for construction industries, in: Proceedings of the CSBE/SCGAB, Edmonton, AB Canada, July 16-19 (July 16-19) (2006) 2006.
[35] J. Page, F. Khadraoui, M. Boutouil, M. Gomina, Multi-physical properties of a structural concrete incorporating short flax fibers, Constr. Build. Mater. 140 (2017) 344–353.
[36] G. Lazorenko, A. Kasprzhitskii, V. Yavna, V. Mischinenko, A. Kukharskii, A. Kruglikov, A. Kolodina, G. Yalovega, Effect of pre-treatment of flax tows on mechanical properties and microstructure of natural fiber reinforced geopolymer composites, Environ. Technol. Innov. 20 (2020).
[37] M. Mathavan, N. Sakthieswaran, O. Ganesh Babu, Experimental investigation on strength and properties of natural fibre reinforced cement mortar, Mater. Today Proc. 37 (2021) 1066–1070.
[38] I. Van de Weyenberg, T. Chi Truong, B. Vangrimde, I. Verpoest, Improving the properties of UD flax fibre reinforced composites by applying an alkaline fibre treatment, Compos. Part A Appl. Sci. Manuf. 37 (2006) 1368–1376.
[39] J. Page, F. Khadraoui, M. Gomina, M. Boutouil, Hydration of flax fibre-reinforced cementitious composites: influence of fibre surface treatments, Eur. J. Environ. Civ. Eng. 26 (2021) 5798–5820.
[40] S. Yang, D. Zheng, C.S. Poon, H. Cui, In-situ alkali–silica reaction evolution of lightweight aggregate concretes prepared with alkali-activated cement and ordinary portland cement assessed by X-ray micro computed-tomography, Cem. Concr. Compos. 140 (2023).
[41] M.K. Mohan, A.V. Rahul, J.F. Van Stappen, V. Cnudde, G. De Schutter, K. Van Tittelboom, Assessment of pore structure characteristics and tortuosity of 3D printed concrete using mercury intrusion porosimetry and X-ray tomography, Cem. Concr. Compos. 140 (2023).
[42] Afnor, Saga Web for ESTP: NF EN 196-1, E: Methods of Testing Cement – Part 1: Determination of Strength, (2006).
[43] N. Afnor, Test methods for mortar in masonry - Part 3: determination of consistence of fresh mortar (by flow table), NF EN 1015 (3) (1999) 12–303.
[44] S. Guessasma, S. Belhabib, Effect of the printing angle on the microstructure and tensile performance of iron-reinforced polylactic acid composite manufactured using fused filament fabrication, J. Manuf. Mater. Process. 8 (2024).

[45] E. Richely, S. Durand, A. Melelli, A. Kao, A. Magueresse, H. Dhakal, T. Gorshkova, F. Callebert, A. Bourmaud, J. Beaugrand, S. Guessasma, Novel insight into the intricate shape of flax fibre lumen, Fibers 9 (2021) 24.
[46] ABQ, (In french) Guide de bonnes pratiques pour l'utilisation des fibres dans le béton, Association béton Québec, 2005, 38.
[47] ACI, State-of-the-Art Report on Fiber Reinforced Concrete, Acids Comm. 544 (2001) 66.
[48] N. Mostefai, R. Hamzaoui, S. Guessasma, A. Aw, H. Nouri, Microstructure and mechanical performance of modified hemp fibre and shiv mortars: discovering the optimal formulation, Mater. Des. 84 (2015) 359–371.
[49] R.J. Müller, A. Steinbüchel, Biodegradability of polymers: regulations and methods for testing, Biopolymers (2002).
[50] L. Rajeshkumar, P.S. Kumar, M. Ramesh, M.R. Sanjay, S. Siengchin, Assessment of biodegradation of lignocellulosic fiber-based composites – A systematic review, Int. J. Biol. Macromol. 253 (2023).
[51] S. Muniyasamy, O. Ofosu, B. Thulasinathan, A.S. Thondi Rajan, S.M. Ramu, S. Soorangkattan, J.B. Muthuramalingam, A. Alagarsamy, Thermal-chemical and biodegradation behaviour of alginic acid treated flax fibres/ poly(hydroxybutyrate-co-valerate) PHBV green composites in compost medium, Biocatal. Agric. Biotechnol. 22 (2019).
[52] B. Crawford, S. Pakpour, N. Kazemian, J. Klironomos, K. Stoeffler, D. Rho, J. Denault, A. Milani, Effect of fungal deterioration on physical and mechanical properties of hemp and flax natural fiber composites, Materials 10 (2017).
[53] S. Ajouguim, M. Stefanidou, K. Abdelouahdi, M. Waqif, L. Saàdi, Influence of treated bio-fibers on the mechanical and physical properties of cement mortars, Eur. J. Environ. Civ. Eng. 26 (2020) 3120–3135.
[54] A. Wongsa, R. Kunthawatwong, S. Naenudon, V. Sata, P. Chindaprasirt, Natural fiber reinforced high calcium fly ash geopolymer mortar, Constr. Build. Mater. 241 (2020).
[55] M. Kurpińska, M. Pawelska-Mazur, Y. Gu, F. Kurpiński, The impact of natural fibers' characteristics on mechanical properties of the cement composites, Sci. Rep. 12 (2022).
[56] J.B. de Oliveira Libório Dourado, M.E.R. Alves, W.A. de Oliveira Júnior, B.L.M. de Oliveira, H. de Jesus Bezerra da Silva, A. López-Galindo, C. Viseras, M.B. Furtini, V. B. dos Santos, Babassu fibers as green mortar additives, J. Nat. Fibers 20 (2023).